International Journal of Innovative Computing, Information and Control
Volume **22**, Number **1**, February **2026**

ICIC International ©2026 ISSN 1349-4198
pp. 5–29

FAULT TOLERANCE CONTROL OF AN ELECTRIC VEHICLE WITH DISTRIBUTED HUB MOTOR UNDER EMB FAILURE CONDITION

Xin Ye[1], Xingang Li[2,*], Xiaoxuan Cheng[1], Qi Cao[3] and Zhongping Kang[1]

[1]School of Vehicle Engineering
Chongqing University of Technology
No. 69, Hongguang Avenue, Banan District, Chongqing 400054, P. R. China
yexin@cqut.edu.cn; { chengxx; kzp }@stu.cqut.edu.cn

[2]Geely Automobile Research Institute (Ningbo) Co., Ltd.
No. 818, Binhai 2nd Road, Hangzhou Bay New District, Ningbo 315336, P. R. China
*Corresponding author: Xingang.Li@geely.com

[3]Joint Logistics Support Force University of Engineering
No. 20, Beiyi Road, Shapingba District, Chongqing 401331, P. R. China
roy1976@163.com

Received April 2025; revised July 2025

Abstract. *Braking performance serves as a fundamental pillar of vehicular operational safety. This paper conducts research on fault-tolerant control for the Electronic Mechanical Brake (EMB) system of distributed In-Wheel Motor Electric Vehicles (IWMEVs) to address potential failures. Firstly, 10 major failure modes and 126 specific failure cases within the EMB system of distributed IWMEVs are identified and analyzed. Subsequently, tailored fault-tolerant controllers are designed for each failure case, leveraging the combined compensation capabilities of in-wheel motors, healthy EMBs, and active steering to mitigate the loss of braking force and ensure braking safety. Finally, we develop a co-simulation platform combining Carsim and Simulink to validate control efficacy across progressive failure scenarios (mild, moderate, and severe). Simulation results demonstrate that the proposed fault-tolerant controllers effectively maintain braking stability, shorten braking distances, and minimize brake pull-to-one-side when EMB failures occur, thereby ensuring braking safety.*

Keywords: Fault-tolerant control, EMB, Hub motor, Braking safety

1. **Introduction.** In electric vehicle system design, optimizing energy recovery while ensuring operational safety presents a fundamental engineering challenge. Regenerative braking captures and recycles energy that would otherwise be lost as heat due to mechanical friction during deceleration or braking. This process enhances energy efficiency, reduces emissions, and extends the vehicle's driving range. Electric vehicles equipped with hub motors and EMB control feature a compact structure, high transmission efficiency, and simplified control, enabling a significant enhancement in regenerative braking efficiency. However, the EMB system lacks an energy storage device, and in the event of a failure, it may partially or completely lose braking force, posing a risk to braking safety. Research in this field mainly focuses on aspects such as sensor faults, actuator faults, fault-tolerant control algorithms, and EMB fault scenarios.

In the research on the fault-tolerant control strategies for sensor failures, Kang [1] studied sensor fault diagnosis and fault tolerance control. Xiao [2] proposed the fundamental strategy for faulft-tolerant motion control based on cooperative game theory to achieve

DOI: 10.24507/ijicic.22.01.5

comprehensive fault tolerance in vehicle motion. Zhu et al. [3] designed fault-tolerant control methods incorporating both software and hardware redundancy to address current sensor failures, thereby improving the reliability of intelligent vehicle braking systems. Dang [4] explored sensor fault diagnosis and fault-tolerant control based on system sensor safety mechanisms, successfully achieving fault-tolerant braking control after sensor failure while meeting the functional safety requirements of braking systems. Some scholars have applied fault-tolerant control methods for nonlinear brake systems to addressing challenging issues such as accurate modeling, reliable fault detection and control design capable of compensating for potential sensor faults [5]. The aforementioned research highlights that these control strategies significantly enhance response speed and efficiency while ensuring control safety.

Focusing on fault-tolerant control for actuator failures, Yuan [6] designed an integral sliding mode fault-tolerant controller for the safety failure risk of linear control dynamic systems. Their approach resolved the virtual control input issue and overcame the challenge of ensuring stability in classical sliding mode controllers when approaching certain quadrants. Qie [7] built a model of compound braking and fault-tolerant control strategy for a motor-driven vehicle with a 16×10-wheel configuration, effectively enhancing braking stability. Patan and Patan [8] proposed a method leveraging the repeatability of control tasks in magnetic braking systems, introducing a comprehensive iterative learning process that includes system identification, fault estimation, and fault-tolerant control. Numerical simulations were conducted to analyze the reference tracking problem in electromagnetic braking systems under various fault scenarios. Raveendran et al. [9] proposed a fault-tolerant controller to overcome vehicle directional instability caused by braking failure. Two sliding mode controllers, differential braking control and steering angle control, were developed to control yaw angle. Cao et al. [10] proposed a Fault-Tolerant Control (FTC) strategy for autonomous vehicle path tracking under brake actuator failure. They designed a fault model and computed a synthetic fault coefficient for the Electro-Hydraulic Braking (EHB) system under differential braking. The proposed strategy enhances vehicle stability and safety across various fault scenarios. Similarly, Yuan et al. [11] proposed a fault-tolerant braking strategy for in-wheel motor-driven electric vehicles based on integral sliding mode control and optimal online distribution. Their approach enables real-time braking force distribution and redistribution, maximizing energy efficiency while isolating faulty actuators, thereby ensuring vehicle stability. While various algorithms have been proposed to enhance vehicle safety at both software and hardware levels, challenges remain. These include computational complexity, the need for improved response speed and accuracy, and the limited scope of failure conditions considered.

In terms of fault-tolerant control algorithms, Wang et al. [12] addressed the challenge of aerodynamic characteristic changes caused by structural failures in aircraft control surfaces. They proposed an adaptive disturbance rejection method based on real-time identification of nonlinear recursive least squares and dynamic inverse control, which significantly improved control stability and response speed and reduced the overshoot. To address power grid fluctuations caused by the uncoordinated charging and discharging of electric vehicles in park microgrids, Yu et al. [13] proposed a charging and discharging strategy based on an improved pigeon flock optimization algorithm incorporating quantum behavior. This method effectively achieved coordinated regulation, enhancing power grid stability while optimizing user benefits. For vehicle platoon control under Denial-of-Service (DoS) attacks on in-vehicle networks, Liu et al. [14] proposed an event-triggered resilient distributed control strategy. Simulations and experiments have verified the effectiveness of this method in maintaining a safe inter-vehicle distance and speed synchronization.

In the context of the EMB failure scenario, Li [15] and his colleagues utilized the torque redistribution capability of the hub motor to compensate for the loss of braking force. At the upper level, Model Predictive Control (MPC) was adopted to optimize the longitudinal dynamics, while at the lower level, motor torque was dynamically adjusted through sliding mode control. Similarly, Wang et al. [16] designed an integrated framework for fault diagnosis and fault tolerance based on an adaptive observer. By dynamically allocating hub motor torque and the braking force of healthy brakes, this approach compensates for the torque loss caused by the EMB failure. The Lyapunov stability theory is introduced to ensure the system convergence. Zhang et al. [17] addressed partial EMB failures by formulating motor torque compensation and residual braking force as a multi-objective optimization problem, employing the Nash equilibrium solution to balance vehicle stability and energy efficiency. Guo et al. [18] were the first to apply Deep Reinforcement Learning (DRL) to EMB fault-tolerant control, designing a decision-making network based on the Actor-Critic framework to dynamically adjust hub motor output in response to sudden braking force changes. Chen et al. [19] proposed an integrated chassis control strategy that considers EMB failure, motor torque saturation, and tire force constraints. Using Nonlinear Model Predictive Control (NMPC), this approach achieved coordinated optimization of longitudinal, lateral, and vertical dynamics. The above-mentioned scholars adopted a hierarchical control framework (upper-level optimization + lower-level execution) and combined it with mainstream methods such as Model Predictive Control (MPC) and sliding mode control to deal with single/double-point faults. However, it is necessary to extend this approach to the extreme situation where both the EMB and the motor fail simultaneously.

To address the braking safety challenges caused by brake system failures in electric vehicles with distributed hub motors, the main contribution of this paper lies in establishing a complex fault-tolerant mechanism for different motor failure scenarios in the brake system of distributed hub motor electric vehicles. The main contents are as follows. First, the EMB and vehicle are accurately modeled to establish the foundation for the subsequent fault-tolerant controller. Then, the fault-tolerant control strategy is designed based on the characteristics of distributed hub motor electric vehicles, which allow independent driving and braking for a single wheel. This strategy is further optimized to account for complex driving scenarios and diverse failure cases. Finally, the motor and health brake compensate for the braking force lost due to the faulty brake, effectively reducing yaw moments caused by braking force imbalances and enhancing overall braking safety and stability.

2. **Failure Cases Analysis of a Distributed Hub Motor Electric Vehicle.**

Reliability is a critical feature of the hydraulic-by-wire braking system, as any failure could lead to severe, even irreversible, consequences for the safety of the driver and passengers. To improve the reliability of the electronic mechanical braking system, we first analyze the failure cases of distributed hub motor electric vehicles.

2.1. **Dynamics modeling of a distributed hub motor electric vehicle.**

The research object of this paper is a distributed hub motor electric vehicle. To comprehensively capture the motion characteristics of all four wheels in three directions, we adopt the 7-degree-of-freedom vehicle model, including the vehicle's longitudinal motion, lateral motion, yaw motion, and rotational motion of the four wheels in the XY plane. The force analysis of this 7-degree-of-freedom vehicle model is shown in Figure 1.

In Figure 1, X is the vehicle's longitudinal coordinate, Y is the vehicle's lateral coordinate, O is the mass center of the vehicle, and β is the slip angle of the mass center

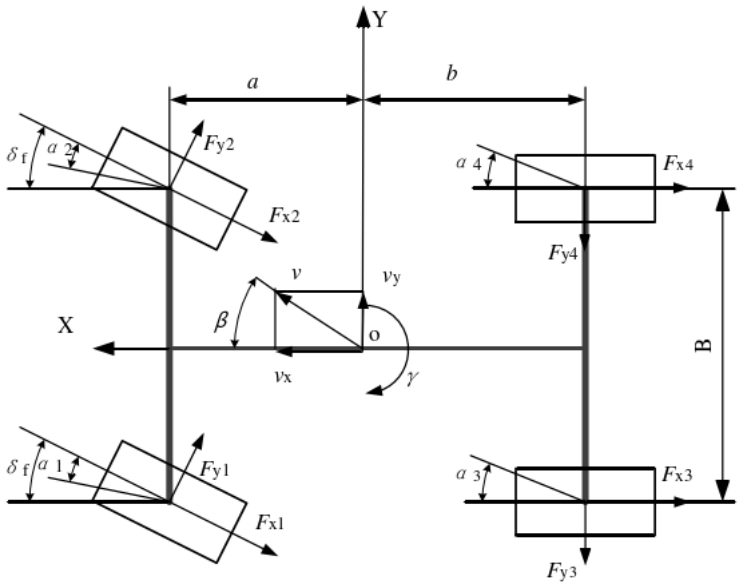

FIGURE 1. Force diagram of the 7-degree-of-freedom vehicle model

(°). According to the force diagram of the 7-DOF vehicle model in Figure 1, the vehicle equilibrium equation on the x-axis, on the y-axis, and around the vertical direction can be expressed as

$$\begin{cases} ma_x = m(\dot{v}_x - v_y\gamma) = (F_{x1} + F_{x2})\cos\delta_f + (F_{y1} + F_{y2})\sin\delta_f + (F_{x3} + F_{x4}) \\ ma_y = m(\dot{v}_y - v_x\gamma) = (F_{y1} + F_{y2})\cos\delta_f - (F_{x1} + F_{x2})\sin\delta_f + (F_{x3} + F_{x4}) \\ M_z = I_z\gamma = a[(F_{x1} + F_{x2})\sin\delta_f - (F_{y1} + F_{y2})\cos\delta_f] - b(F_{x3} + F_{x4}) \end{cases} \tag{1}$$

where γ is yaw velocity (deg/s), v is actual vehicle speed (m/s), a and b are the distances from the vehicle mass center to the front and rear axles, respectively (m), B is the wheelbase (m), δ_f is the rotational angle of the front wheel (°), a_1, a_2, a_3 and a_4 are the sideslip angles of each wheel, respectively (°). F_{xi} and F_{yi} denote longitudinal and lateral forces of the ith wheel, respectively (N), m is the vehicle's mass (kg), a_x is the longitudinal acceleration (m/s^2); a_y is the lateral acceleration (m/s^2); $\dot{v}_x$ is the derivative of the longitudinal velocity component on the mass center (m/s^2), $\dot{v}_y$ is the derivative of the lateral velocity component on the mass center (m/s^2), and $\dot{v}_y = \dot{v}_x * \dot{\beta}$. I_z denotes yaw moment of inertia (kg·m^2).

Based on the aforementioned dynamic model of electric vehicles with distributed hub motors, we conduct an analysis of the failure cases of the hub motors during straight-line braking for distributed electric vehicles. Taking account of the compensatory capability of the remaining torque of the motors, we primarily discussed two scenarios: single-wheel failure and double-wheel failure. These two scenarios include 10 major failure modes, consisting of 4 types of hub motor failures in the left front wheel, right front wheel, left rear wheel, and right rear wheel, and 6 types of hub motor failures in two front wheels, two rear wheels, two left wheels, two right wheels, left front and right rear wheels, and right front and left rear wheels. For each failure mode, according to different degrees of braking force loss, it is further subdivided into 126 failure cases (Arabic numerals: 1, 2, 3, ...), and these judgment conditions are defined for each failure case (Uppercase English letters: A, B, C, ...).

2.2. **Single-wheel failure during straight-line braking.** The single-wheel failure cases during straight-line braking are classified into four types: left front wheel failure, right

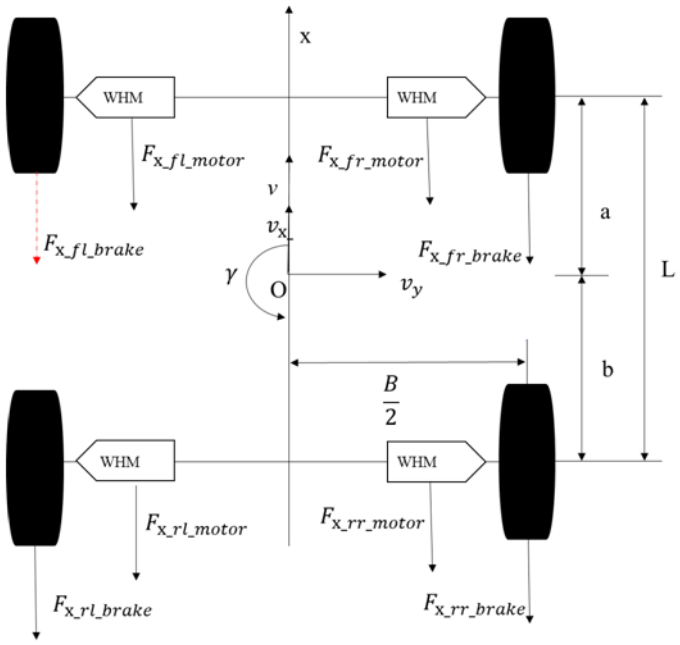

FIGURE 2. Force analysis diagram of the left front wheel failure

front wheel failure, left rear wheel failure, and right rear wheel failure. During high-speed braking, these four single-wheel failure cases can pose a significant safety hazard to the vehicle. This subsection analyzes the failure of the left front wheel as an example, with Figure 2 displaying the force analysis.

In Figure 2, $F_{x\_fl\_motor}$, $F_{x\_fr\_motor}$, $F_{x\_rl\_motor}$ and $F_{x\_rr\_motor}$ represent the hubmotor braking force of the left front wheel, right front wheel, left rear wheel, and right rear wheel, respectively (N). $F_{x\_fl\_brake}$, $F_{x\_fr\_brake}$, $F_{x\_rl\_brake}$ and $F_{x\_rr\_brake}$ are the brake forces on the left front wheel, the right front wheel, the left rear wheel, and the right rear wheel, respectively (N). L is the wheelbase (m). When the left front wheel brake fails, i.e., $F_{x\_fl\_brake}$ is partially or completely lost, the ground braking force for each wheel is shown in Equation (2):

$$\begin{cases} F_{x\_fl} = F_{x\_fl\_motor} + F_{x\_fl\_brake\_b} \\ F_{x\_fr} = F_{x\_fr\_motor} + F_{x\_fr\_brake} \\ F_{x\_rl} = F_{x\_rl\_motor} + F_{x\_rl\_brake} \\ F_{x\_rr} = F_{x\_rr\_motor} + F_{x\_rr\_brake} \end{cases} \tag{2}$$

where $F_{x\_fl\_brake\_b}$ denotes the remaining braking force after the left front wheel failure (N). F_{x_fl}, F_{x_fr}, F_{x_rl} and F_{x_rr} are the ground braking forces of the left front wheel, the right front wheel, the left rear wheel, and the right rear wheel, respectively (N).

When the left front wheel fails, the vehicle's yaw velocity is shown in Equation (3):

$$I_z\gamma = a[(F_{x1} + F_{x2})\sin\delta_f - (F_{y1} + F_{y2})\cos\delta_f] - b(F_{x3} + F_{x4}) \tag{3}$$

The degree of wheel failure is classified into three levels: mild failure, moderate failure, and severe failure, as detailed in Table 1.

TABLE 1. Failure analysis table for the left front wheel

Judgment condition	A	B	C	D
Failure cases	1	2	3	4
Degree of failure	Mild failure	Moderate failure		Severe failure

In this case, mild failure means that the braking force loss is less than the effective maximum regenerative braking force of the hub motor on the same wheel, as shown in condition A of Equation (4). Moderate failure consists of two cases: one is that the braking force loss is greater than the effective regenerative braking force of the hub motor on the same wheel and less than the total effective braking force of the hub motors of the two wheels on the same side, as shown in condition B of Equation (4), and the other is that the braking force loss is greater than the total effective braking force of the hub motors of the two wheels on the same side and less than the sum of the remaining mechanical braking forces of the two wheels on the same side, as shown in condition C of Equation (4). Severe failure is defined as a braking force loss greater than the sum of the remaining mechanical braking forces of the two wheels on the same side, as shown in condition D of Equation (4). The above four cases in Table 1 correspond to Nos. 1-4, representing four failure scenarios. We discriminate the braking force loss of the left front wheel using the four judgment conditions A∼D in Equation (4):

$$\begin{cases} \text{A: } F_{x\_fl\_brake\_loss} \leq F_{x\_fl\_motor\_re} \\ \text{B: } F_{x\_fl\_motor\_re} < F_{x\_fl\_brake\_loss} \leq F_{x\_l\_motor\_re} \\ \text{C: } F_{x\_l\_motor\_re} < F_{x\_fl\_brake\_loss} \leq F_{x\_l\_brake\_re} \\ \text{D: } F_{x\_l\_brake\_re} < F_{x\_fl\_brake\_loss} \end{cases} \tag{4}$$

where $F_{x\_fl\_brake\_loss}$ is the braking force loss of the brake on the left front wheel (N), $F_{x\_fl\_motor\_re}$ is the remaining braking force of the motor on the left front wheel (N), $F_{x\_l\_motor\_re}$ is the sum of the remaining braking forces of the front and rear motors on the left side (N), and $F_{x\_l\_brake\_re}$ is the sum of the remaining braking forces of the front and rear brakes on the left side (N).

In the event of a single-wheel failure, the mechanical model analysis, yaw rate calculation model, and failure condition assessment for the right front wheel, right rear wheel, and left rear wheel failures can be analogously derived by referencing the analytical approach used in the left front wheel failure case.

2.3. **Two-wheel failure during straight-line braking.** Compared to a single-wheel failure, a two-wheel failure leads to a significant increase in braking distance due to the greater loss of braking force and the challenge of meeting the required driving force. Additionally, the imbalance in braking force between the two failed wheels further heightens the risk of vehicle instability. In the scenario of double-wheel failure, the degree of failure depends on the wheel with the most severe braking force loss. For example, if the left front wheel has slight failure and the right rear wheel has severe failure, then the failure degree of two-wheel in this case is defined as severe failure.

2.3.1. *Front/rear axle two-wheel failure during straight-line braking.* Coaxial double-wheel failure includes two situations: double-wheel failure of the front axle and two-wheel failure of the rear axle. Both cases require consideration of two factors: the magnitude of the braking force loss on the left and right wheels of the same axle, and the total change in braking force. This subsection takes an example of the simultaneous brake failure of two wheels on the front axle and analyzes its failure. As shown in Figure 2, i.e., $F_{x\_fl\_brake}$, $F_{x\_fr\_brake}$ partially lost. The braking force of each wheel is

$$\begin{cases} F_{x\_fl} = F_{x\_fl\_motor} + F_{x\_fl\_brake\_b} \\ F_{x\_fr} = F_{x\_fr\_motor} + F_{x\_fr\_brake\_b} \\ F_{x\_rl} = F_{x\_rl\_motor} + F_{x\_rl\_brake} \\ F_{x\_rr} = F_{x\_rr\_motor} + F_{x\_rr\_brake} \end{cases} \tag{5}$$

where $F_{x\_fr\_brake\_b}$ is the remaining braking force of the brake on the right front wheel after failure (N). At this time, the vehicle's yaw velocity is the same as shown in Equation (3).

The analysis identifies 16 distinct failure cases associated with front/rear axle two-wheel failure, with the judgment conditions outlined in Equation (4) and Equation (6). Based on these criteria, the failure cases are sequentially numbered from Nos. 5 to 20, as detailed in Table 2.

$$\begin{cases} \text{E: } F_{x\_fr\_brake\_loss} \le F_{x\_fr\_motor\_re} \\ \text{F: } F_{x\_fr\_motor\_re} < F_{x\_fr\_brake\_loss} \le F_{x\_r\_motor\_re} \\ \text{G: } F_{x\_r\_motor\_re} < F_{x\_fr\_brake\_loss} \le F_{x\_r\_brake\_re} \\ \text{H: } F_{x\_r\_brake\_re} < F_{x\_fr\_brake\_loss} \end{cases} \tag{6}$$

where $F_{x\_fr\_brake\_loss}$ is the braking force loss of the brake on the rear front wheel (N), $F_{x\_fr\_motor\_re}$ is the remaining braking force of the motor on the right front wheel (N), $F_{x\_r\_motor\_re}$ is the remaining braking force of the front and rear motors on the right side (N), $F_{x\_r\_brake\_re}$ is the remaining braking force of the front and rare brakes on the right side (N).

Table 2. Failure analysis table for the left front wheel and right front wheel

Failure cases	A	B	C	D
E	5	6	7	8
F	9	10	11	12
G	13	14	15	16
H	17	18	19	20

As illustrated in Table 2, failure case No. 5 satisfies A and E, representing mild failure; failure cases Nos. 9 and 13 satisfy A, F and A, G, respectively, representing moderate failure; and failure case No. 17 satisfies conditions A and H, representing severe failure. Double-wheel failure on the rear axle refers to two-wheel failure on the front axle.

2.3.2. *The failure of two diagonal wheels during straight-line braking.* The failure of two diagonal wheels is more complex than that of coaxial double-wheel failure. It needs to consider both the loss of braking force in the two failed wheels and the compensation provided by the remaining wheels on the same axle. In this subsection, the failure case analysis is carried out by taking the example of the simultaneous braking failure of both the left front wheel and right rear wheel, as shown in Figure 2, i.e., partial or total loss of $F_{x\_fl\_brake}$, $F_{x\_rr\_brake}$. The braking force of each wheel is shown in Equation (7):

$$\begin{cases} F_{x\_fl} = F_{x\_fl\_motor} + F_{x\_fl\_brake\_b} \\ F_{x\_fr} = F_{x\_fr\_motor} + F_{x\_fr\_brake} \\ F_{x\_rl} = F_{x\_rl\_motor} + F_{x\_rl\_brake} \\ F_{x\_rr} = F_{x\_rr\_motor} + F_{x\_rr\_brake\_b} \end{cases} \tag{7}$$

where $F_{x\_rr\_brake\_b}$ is the brake force on the right rare wheel after failure (N). The lateral swing angular velocity of this vehicle is the same as shown in Equation (3).

As Table 3 contains 16 kinds of failure cases, according to the judgment conditions of Equation (4) and Equation (8), the brake failure cases are numbered according to Nos. 21∼36, as shown in Table 3.

$$\begin{cases} \text{I: } F_{x\_rr\_brake\_loss} \le F_{x\_rr\_motor\_re} \\ \text{J: } F_{x\_rr\_motor\_re} < F_{x\_rr\_brake\_loss} \le F_{x\_r\_motor\_re} \\ \text{K: } F_{x\_r\_motor\_re} < F_{x\_rr\_brake\_loss} \le F_{x\_r\_brake\_re} \\ \text{L: } F_{x\_r\_brake\_re} < F_{x\_rr\_brake\_loss} \end{cases} \tag{8}$$

where $F_{x\_rr\_brake\_loss}$ is the loss of braking force caused by the failure of the right rear wheel (N), $F_{x\_rr\_motor\_re}$ is the remaining braking force of the motor on the right rare wheel, (N).

TABLE 3. Failure analysis table for the left front wheel and the right rear wheel

Failure cases	A	B	C	D
I	21	22	23	24
J	25	26	27	28
K	29	30	31	32
L	33	34	35	36

As illustrated in Table 3, the failure case No. 21 satisfies conditions A and I, representing mild failure; failure cases Nos. 25 and 29 satisfy conditions A, J, and A, K, respectively, representing moderate failure; and failure case No. 33 satisfies conditions A and L, representing severe failure. Based on the above analysis, we can establish the failure of two diagonal wheels in the opposite direction.

2.3.3. *Two-wheel failure on the same side during straight-line braking.* Two-wheel failure on the same side is the most dangerous failure case. As illustrated in Figure 2, such a failure not only drastically reduces braking force and compromises vehicle stability but also eliminates the possibility of compensating for the lost braking force with the wheels on the same side. This sub-section provides an example of the simultaneous braking failure of both the left front and left rear wheels. The failure analysis is carried out, as shown in Figure 2, $F_{x\_fl\_brake}$ and $F_{x\_rl\_brake}$ partly or completely lost. The braking force of each wheel is shown in Equation (9). The vehicle yaw velocity is the same as shown in Equation (3).

$$\begin{cases} F_{x\_fl} = F_{x\_fl\_motor} + F_{x\_fl\_brake\_b} \\ F_{x\_fr} = F_{x\_fr\_motor} + F_{x\_fr\_brake} \\ F_{x\_rl} = F_{x\_rl\_motor} + F_{x\_rl\_brake\_b} \\ F_{x\_rr} = F_{x\_rr\_motor} + F_{x\_rr\_brake} \end{cases} \tag{9}$$

where $F_{x\_rl\_brake\_b}$ is the brake force of the left rear wheel after failure, (N).

Table 4 contains 25 different failure cases, which are numbered from Nos. 37 to 61 based on the judgment criteria outlined in Equation (4) and Equation (10).

$$\begin{cases} \text{M: } F_{x\_rl\_brake\_loss} \le F_{x\_rl\_motor\_re} \\ \text{N: } F_{x\_rl\_motor\_re} < F_{x\_rl\_brake\_loss} \le F_{x\_l\_motor\_re}, F_{x\_rl\_brake\_loss} + F_{x\_fl\_brake\_loss} \le F_{x\_l\_motor\_re} \\ \text{O: } F_{x\_rl\_motor\_re} < F_{x\_rl\_brake\_loss} \le F_{x\_l\_motor\_re}, F_{x\_rl\_brake\_loss} + F_{x\_fl\_brake\_loss} > F_{x\_l\_motor\_re} \\ \text{P: } F_{x\_l\_motor\_re} < F_{x\_rl\_brake\_loss} \le F_{x\_l\_brake\_re} \\ \text{Q: } F_{x\_l\_brake\_re} < F_{x\_rl\_brake\_loss} \\ \text{R: } F_{x\_fl\_motor\_re} < F_{x\_fl\_brake\_loss} \le F_{x\_l\_motor\_re}, F_{x\_rl\_brake\_loss} + F_{x\_fl\_brake\_loss} \le F_{x\_l\_motor\_re} \\ \text{S: } F_{x\_fl\_motor\_re} < F_{x\_fl\_brake\_loss} \le F_{x\_l\_motor\_re}, F_{x\_rl\_brake\_loss} + F_{x\_fl\_brake\_loss} > F_{x\_l\_motor\_re} \end{cases} \tag{10}$$

where $F_{x\_rl\_brake\_loss}$ is the loss of braking force caused by the failure of the left rear wheel, (N); $F_{x\_rl\_motor\_re}$ is the remaining braking force of the motor on the left rear wheel, (N).

As illustrated in Table 4, the failure case No. 37 satisfies conditions A and M, representing mild failure; the failure case No. 42 satisfies conditions A and N, representing moderate failure; and the failure cases Nos. 47, 52, and 57 satisfy conditions A, O, A, P, and A, Q, respectively, representing severe failure. Based on the above analysis, it is also possible to establish a two-wheel failure case on the right side.

TABLE 4. Failure analysis table for the left front wheel and the left rare wheel

Failure cases	A	R	S	C	D
M	37	38	39	40	41
N	42	43	44	45	46
O	47	48	49	50	51
P	52	53	54	55	56
Q	57	58	59	60	61

3. Fault-Tolerant Control Strategy Design.

3.1. EMB model construction.

The EMB system includes a torque motor, a reduction gearing, opposite-turning ball screw pair, brake friction blocks and brake discs. The ball screw features oppositely threaded nuts, as illustrated in Figure 3. When activated, the motor rotates, driving the ball screw and nuts apart, which in turn pushes the brake pads evenly toward the disc. This mechanism ensures consistent friction and smooth control.

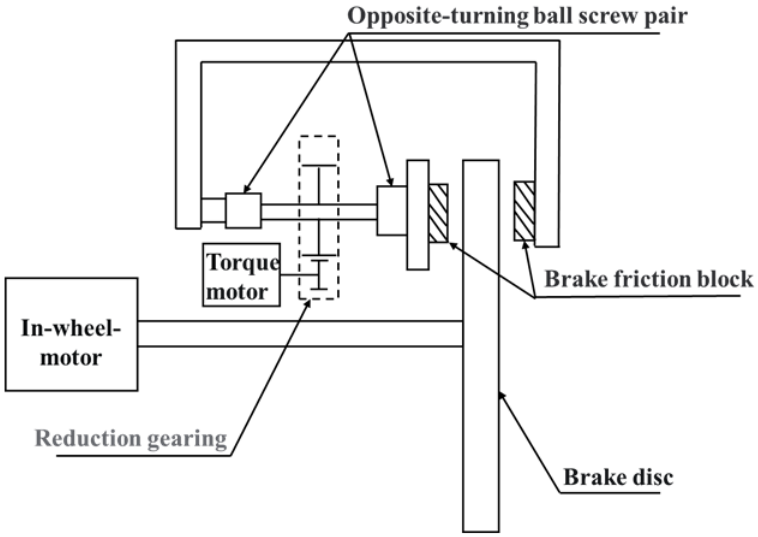

FIGURE 3. Structure of EMB

Referring to the pressure design of the hydraulic brake system, the maximum clamping force of the EMB system is 30 kN [20], and the relationship between the driving force of the ball screw shaft and the clamping force of the brake piece is

$$T_c = F_{cl}\frac{d_m}{2}\tan(\lambda + \rho') \tag{11}$$

where T_c is the clamping force of the brake piece, (Nm); F_{cl} is the driving force of the ball screw shaft, (N); d_m is the nominal diameter, (mm); λ is the helix angle, (°); ρ' is the friction angle of equivalent weight, (°). Equation (11), which matches the ball screw shaft parameters and torque motor parameters of the EMB system, designs the gear ratio of the gear reduction mechanism to be $i = 15$.

To meet the high torque and precision requirements of the EMB system, a torque motor is chosen as the power source. This motor provides a high torque output and enables more accurate control, ensuring reliable braking performance.

The first step involves performing the necessary calculations for the torque motor. The operating circuit of a DC torque motor consists of resistors and inductors connected in series, as shown in Figure 4. The armature voltage $u_a(t)$ is input into the circle, generating

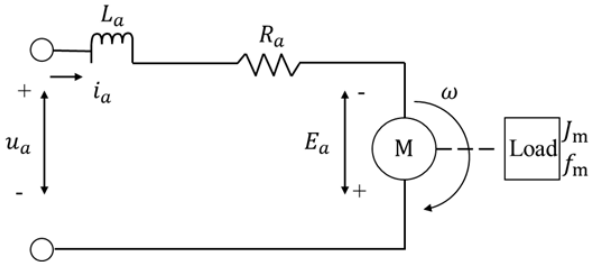

FIGURE 4. Working principal diagram of DC torque motor

a current $i_a(t)$ in the armature loop. The current $i_a(t)$ interacts with the excitation magnetic flux to produce an electromagnetic torque $T_m(t)$, which drives the load into motion.

The voltage balance equation of the armature loop is obtained from Kirchhoff's law:

$$u_a(t) = L_a \frac{di_a(t)}{dt} + R_a i_a(t) + E_a \tag{12}$$

where $u_a(t)$ is armature voltage, (V); L_a is inductance, (H); $i_a(t)$ is current, (A); R_a is internal resistance, (Ω); E_a is terminal voltage, (V).

Electromagnetic torque equation:

$$T_m(t) = K_T i_a(t) \tag{13}$$

where $T_m(t)$ is the electromagnetic torque, (Nm); K_T is the torque coefficient, (Nm-A^{-1}).

The torque balance equation of the motor output shaft is

$$J_m \frac{d\omega(t)}{dt} + f_m \omega(t) = T_m(t) - T_L(t) \tag{14}$$

where $T_L(t)$ is the load torque, (Nm); f_m is the viscous friction coefficient, (N/m^2); $\omega(t)$ is the angular velocity, (rad/s); J_m is the moment of inertia (kg·m^2).

Using the above equation, we establish the relationship among the load, motor torque, and motor voltage. To facilitate modeling, the next step involves deriving the transfer function based on these relationships. Bringing Equation (12) and Equation (13) into Equation (14) and eliminating the intermediate variables $i_a(t)$, E_a and $T_m(t)$ the differential equation of the DC motor can be obtained as the output $\omega(t)$ and the input $u_a(t)$. Given the circuit's small inductance value, we can disregard it. Consequently, we obtain the simplified differential equation:

$$T_t \frac{d\omega(t)}{dt} + \omega(t) = K_m u_a(t) - K_c T_L(t) \tag{15}$$

where K_m is the motor time constant, $K_m = K_T/(R_a f_m + K_T K_E)$; K_c is the motor transfer coefficient, $K_c = R_a/(R_a f_m + K_T K_E)$; T_t is the time constant, (s); K_E is the counter electric potential coefficient (V-r/min^{-1}).

Laplace transformation of Equation (15) is obtained:

$$T_t s\omega(s) + \omega(s) = K_m u_a(s) - K_c T_L(s) \tag{16}$$

According to the superposition principle of transfer functions in linear systems, making $T_L(s) = 0$ can obtain the transfer function $G(s)$ from voltage $u_a(t)$ to angular velocity $\omega(t)$ as

$$G(s) = \frac{\Omega(s)}{U_a(s)} = \frac{K_m}{T_m s + 1} \tag{17}$$

Let $u_a(s) = 0$, and then we get the transfer function $G_m(s)$ from load torque $T_L(t)$ to rotating velocity $\omega_m(t)$ as

$$G_m(s) = \frac{\Omega(s)}{T_L(s)} = \frac{-K_c}{T_m s + 1} \tag{18}$$

The EMB's torque motor achieves linear braking, and the dual-loop PID system enhances responsiveness and accuracy [21]. The outer load loop calculates the real-time clamping force, while the inner speed loop regulates the motor speed, ensuring precise torque output control.

Knowing the load-torque-speed relation, Equation (11) indicates that controlling the motor driving the ball screw requires regulating the clamping force of the brake block. After eliminating clearance, the relationship between the clamping force F_{cl} and the brake block displacement x is expressed as follows [22]:

$$F_{cl} = K_{cl} * x^3 \tag{19}$$

where K_{cl} is the clamping force coefficient.

To obtain the displacement of the brake piece, it is necessary to integrate the angular velocity of the torque motor's output, and the rotational angle is transmitted through the drive system to the radial displacement of the brake block. At this point, the EMB system operates as a second-order system, utilizing voltage as the input and clamping force as the output. We can represent this system using the transfer function as follows:

$$G_{EMB}(s) = [G(s) + G_m(s)] * G_{tran}(s) \tag{20}$$

where $G_{EMB}(s)$ is the transfer function of the EMB system; $G_{tran}(s)$ is the transfer function of the mechanical system.

Based on the mathematical model of the EMB braking system described by the above transfer function, the structure of the EMB system with double closed-loop PID control is shown in Figure 5.

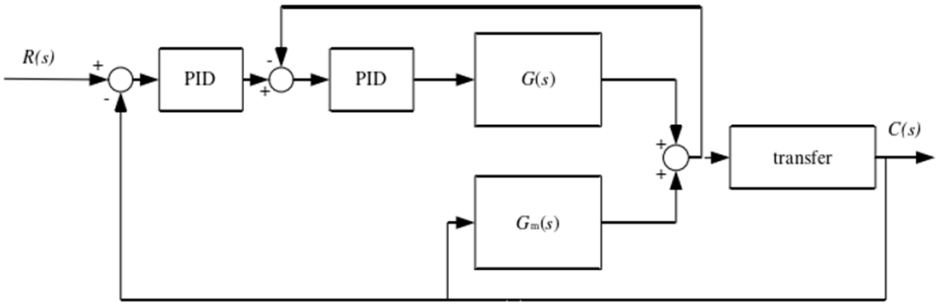

FIGURE 5. The EMB system with double closed-loop PID control

In Figure 5, $R(s)$ is the target braking force of the EMB system; $C(s)$ is the output braking force of the EMB system; $G(s)$ and $G_m(s)$ are shown in Equation (17) and Equation (18). 'transfer' is the transmission function for the process of braking force provided by the EMB self-torque motor torque output through the reducer and the ball screw transmission mechanism to the brake friction block.

3.2. **Fault-tolerant controller design.** This section requires the realization of fault-tolerant control for 10 types of brake failure modes (including 126 failure cases). The design of the controller is related to the force conditions of the front and rear wheels during braking. For simplicity, air resistance and rolling resistance are neglected. To model the system, separate torque balance equations are established for the front and rear wheels:

$$\begin{cases} F_{zf}L = Gb + m\dfrac{du}{dt}h_g \\ F_{zr}L = Ga - m\dfrac{du}{dt}h_g \end{cases} \tag{21}$$

where F_{zf} and F_{zr} are the normal reaction force of the ground acting on the front and rear wheels, respectively, (N); h_g is the height of the vehicle mass center, (m); G is the vehicle gravity, (N). The force applied on the wheels satisfies the relationship of adhesion ellipse, as shown in Figure 6.

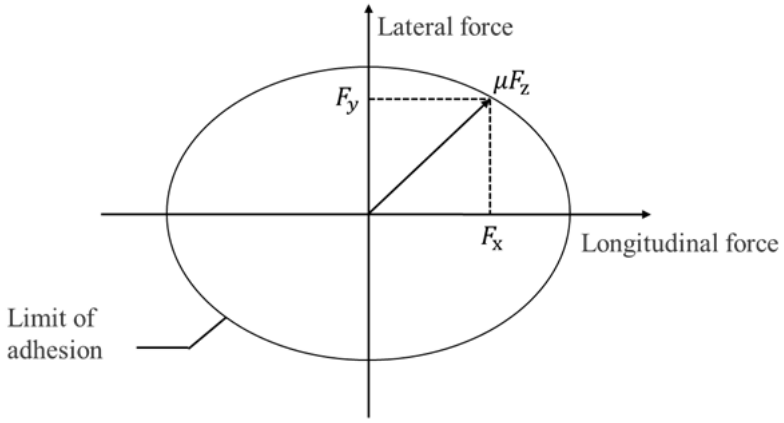

FIGURE 6. The tire adhesion ellipse

When the wheel's vertical load is certain, the longitudinal force and lateral force of this wheel are satisfied

$$\left(\frac{F_x}{\mu F_z}\right)^2 + \left(\frac{F_y}{\mu F_z}\right)^2 \leq 1 \tag{22}$$

$$\begin{cases} F_{x\_fl\_brake\_max} = F_{zf}\mu/2 - F_{x\_fl\_motor\_max} \\ F_{x\_fr\_brake\_max} = F_{zf}\mu/2 - F_{x\_fr\_motor\_max} \\ F_{x\_rl\_brake\_max} = F_{zr}\mu/2 - F_{x\_rl\_motor\_max} \\ F_{x\_rr\_brake\_max} = F_{zr}\mu/2 - F_{x\_rr\_motor\_max} \end{cases} \tag{23}$$

where μ is the pavement adhesion coefficient. Based on the force constraint relationship during the wheel braking process, fault-tolerant designs are carried out for typical failure cases under different failure modes.

3.2.1. *Fault-tolerant control strategy for single-wheel failure.* In the case where only one wheel fails, the control strategy is designed for failure cases Nos. 1 to 4, according to the analysis in Subsection 2.2.

Failure case No. 1 satisfies judgment condition A: $F_{x\_fl\_brake\_loss} < F_{x\_fl\_motor\_re}$, by that the lost braking force is less than the braking force provided by the motor, and the braking force can be compensated by the hub motor on this wheel. The equation is as follows:

$$F_{x\_fl\_motor\_p} = F_{x\_fl\_motor} + F_{x\_fl\_brake\_loss} \tag{24}$$

where $F_{x\_fl\_motor\_p}$ is the output braking force of the motor on the left front wheel, (N).

Failure case No. 2 satisfies judgment condition B: $F_{x\_fl\_motor\_re} < F_{x\_fl\_brake\_loss} < F_{x\_l\_motor\_re}$, in this case, the lost braking force is less than the braking force provided by the motor on the same side, and the braking force could be compensated by the wheel-hub motors on the same side. The equations are as follows:

$$\begin{cases} F_{x\_fl\_motor\_p} = F_{x\_fl\_motor\_max} \\ F_{x\_rl\_motor\_p} = F_{x\_rl\_motor\_max} + F_{x\_fl\_motor\_max} - F_{x\_fl\_motor\_p} - F_{x\_fl\_brake\_loss} \end{cases} \tag{25}$$

where $F_{x\_rl\_motor\_p}$ is the output braking force of the motor on the left rear wheel, (N).

Failure case No. 3 satisfies judgment condition C: $F_{x\_l\_motor\_re} < F_{x\_fl\_brake\_loss} < F_{x\_l\_brake\_re}$, at this time, the lost braking force is less than the sum of the braking force provided by the motors on the same side and EMB, and the braking force can be compensated by the wheel-hub motors on the same side and EMB. The equations are as follows:

$$\begin{cases} F_{x\_fl\_motor\_p} = F_{x\_fl\_motor\_max} \\ F_{x\_rl\_motor\_p} = F_{x\_rl\_motor\_max} \\ F_{x\_rl\_brake\_p} = F_{x\_rl\_brake\_max} + F_{x\_l\_motor\_re} - F_{x\_fl\_brake\_loss} \end{cases} \tag{26}$$

where $F_{x\_rl\_brake\_p}$ is the output braking force of the brake on the left rear wheel, (N).

Failure case No. 4 satisfies judgment condition D: $F_{x\_l\_brake\_re} < F_{x\_fl\_brake\_loss}$, at this point, the lost braking force surpasses the combined braking force from the same side motor and the EMB. This constitutes a severe failure condition, where the braking force deficit cannot be compensated, necessitating active steering control to maintain stability. In order to improve vehicle stability, the steering wheels should be neutralized at this point by giving a rotational angle that could produce yaw velocity in the opposite direction.

This can be achieved using the following equation, where the vehicle yaw velocity serves as the input and the rotational angle of the front wheel is the output. The equation is as follows:

$$m * (\dot{v}_x - v_y * \gamma) = (F_{x1} + F_{x2}) \cos \delta_f + (F_{y1} + F_{y2}) \sin \delta_f + (F_{x3} + F_{x4}) \tag{27}$$

3.2.2. *Fault-tolerant control strategy for two-wheel failure.* According to the analysis in Subsection 2.3, since the front/rear axle two-wheel failure case is similar to the failure of two diagonal wheels, this subsection designs the fault-tolerant control strategy as follows, taking the front-axial two-wheel and the left-side two-wheel failure cases as examples:

(i) Fault-tolerant control strategy for the front/rear axle two-wheel failure. To save space, the fault-tolerant strategies for failure cases No. 5 and No. 14 from Table 2 are selected for description. Failure case No. 5 satisfies judgment conditions A and E. Currently, the two wheels lose less braking force than the motors provide, and the braking force can be compensated by the hub motor on this wheel. The equations are as follows:

$$\begin{cases} F_{x\_fl\_motor\_p} = F_{x\_fl\_motor} + F_{x\_fl\_brake\_loss} \\ F_{x\_fr\_motor\_p} = F_{x\_fr\_motor} + F_{x\_fr\_brake\_loss} \end{cases} \tag{28}$$

where $F_{x\_fr\_motor\_p}$ is the output braking force of the motor on the right front wheel, (N).

Failure case No. 14 satisfies judgment conditions B and G. In this case, the braking force lost by the left front wheel is less than the braking force provided by the motor on the same side, and the braking force lost by the right front wheel is less than the sum of the braking force provided by the motor on the same side and the EMB. The braking force loss of the left front wheel is compensated by the wheel-hub motors on the same side, while the braking force loss of the right front wheel can be compensated by both the wheel-hub motors on the same side and the EMB. The equations are as follows:

$$\begin{cases} F_{x\_fl\_motor\_p} = F_{x\_fl\_motor\_max} \\ F_{x\_rl\_motor\_p} = F_{x\_rl\_motor} + F_{x\_fl\_motor\_max} - F_{x\_fl\_motor\_p} - F_{x\_fl\_brake\_loss} \\ F_{x\_fr\_motor\_p} = F_{x\_fr\_motor\_max} \\ F_{x\_rr\_motor\_p} = F_{x\_rr\_motor\_max} \\ F_{x\_rr\_brake\_p} = F_{x\_rr\_brake\_max} + F_{x\_r\_motor\_re} - F_{x\_fr\_brake\_loss} \end{cases} \tag{29}$$

where $F_{x\_rr\_brake\_p}$ is the output braking force of the brake on the right rear wheel, (N).

Failure cases Nos. 8, 12, 16, 17, 18, 19, and 20 are classified as severe failure cases, which are unable to meet the required braking force. These conditions can be addressed by combining active steering to ensure braking stability. The remaining failure cases are analogous and will not be repeated here.

(ii) Fault-tolerant control strategy for two-wheel failure on the same side. We will describe the situation by taking failure scenarios 37 and 38 from Table 4 as our examples. No. 37 satisfies judgment conditions A and M. In this case, the braking force lost by both wheels is less than the braking force provided by the motors on the same side, and the braking force can be compensated by the hub motor on this wheel. The equations are as follows:

$$\begin{cases} F_{x\_fl\_motor\_p} = F_{x\_fl\_motor} + F_{x\_fl\_brake\_loss} \\ F_{x\_rl\_motor\_p} = F_{x\_rl\_motor} + F_{x\_rl\_brake\_loss} \end{cases} \tag{30}$$

No. 38 satisfies judgment conditions R and M. At this time, the braking force lost by the left rear wheel is less than the braking force provided by the motors on the same side, and the braking force lost by the left front wheel is less than the braking force provided by the motors on the same side; the braking force loss of the left rear wheel is compensated for by the hub motor on this wheel, and the braking force loss of the left front wheel can be compensated for by the wheel-hub motors on the same side. The equations are as follows:

$$\begin{cases} F_{x\_rl\_motor\_p} = F_{x\_rl\_motor\_max} + F_{x\_fl\_motor\_max} - F_{x\_fl\_motor} + F_{x\_rl\_brake\_loss} \\ F_{x\_fl\_motor\_p} = F_{x\_fl\_motor\_max} \\ F_{x\_rl\_brake\_p} = F_{x\_rl\_brake} + F_{x\_rl\_motor\_max} - F_{x\_fl\_motor\_p} \end{cases} \tag{31}$$

Failure cases Nos. 39∼41, 43, 44∼61 are severe failure cases, which cannot satisfy the demand braking force and can be combined with active steering to ensure braking stability. The rest of the failure cases are analogous and will not be repeated.

3.2.3. *Controller stability analysis.* The controller employs high-gain feedback. To verify the stability of the system, the *Lyapunov function* is employed for stability analysis. The differential equation of the nonlinear system is assumed as

$$\dot{x} = ax^2 + u \tag{32}$$

where x is the state of the controlled system; u is the system input (controller output); a indicates the uncertainty of the system. The error function is defined when the control goal is error approaching zero:

$$e = x_d - x \tag{33}$$

where e is the error; x_d is the target value pursued by the system.

Take the derivative of the error function:

$$\dot{e} = \dot{x}_d - \dot{x} = \dot{x}_d - f(x) - u \tag{34}$$

where $f(x)$ is the nonlinear term in the controlled system, ax^2. According to Lyapunov's second method of stability, stable system energy is always dissipated continuously, define a scalar function $V(x)$, which is called Lyapunov stability if $V(x)$ satisfies the following requirements:

1) When $x = 0$, $V(x) = 0$;
2) When $x \neq 0$, $V(x) > 0$;
3) When $x \neq 0$, $\frac{dV(x)}{dt} \leq 0$.

Define the *Lyapunov function* for the above system as

$$V(x) = \frac{1}{2}e^2 \tag{35}$$

It can be seen that the *Lyapunov function* in Equation (34) is positive definite, and its derivative with respect to time is

$$\dot{V}(x) = e * \dot{e} = e * (x_d - f(x) - u),\ |f(x)| < \rho(x) \tag{36}$$

where $\rho(x)$ is the boundary of the nonlinear term of the controlled system. Let the input in Equation (34) be

$$u = \dot{x}_d + ke + u_{aux} \tag{37}$$

where u_{aux} is the control responsible for pulling the system back to the phase plane stability value when it deviates from the expected value. In the controller, the control items are

$$u_{aux} = \frac{1}{\varepsilon}\rho^2 e \tag{38}$$

where ε is a constant greater than 0, which is the parameter adjusted by the designer; ρ is the system boundary. From Equation (36) and Equation (38), ρ is the system boundary, so, $\rho > f(x)$, $\dot{V}(x) \leq -ke^2$ is derived.

High gain robust controller:

$$\dot{V}(x) = -ef(x) - ke^2 - \frac{1}{\varepsilon}\rho^2 e^2 \leq \rho|e| - ke^2 - \frac{1}{\varepsilon}\rho^2 e^2 \tag{39}$$

Equation (39) is obtained by deformation:

$$\dot{V}(x) \leq -ke^2 + \rho|e|\left(1 - \frac{1}{\varepsilon}\rho|e|\right) \tag{40}$$

Equation (40) is divided into two cases depending on the value of ε:
1) $\rho|e| > \varepsilon$

$$|e| > \varepsilon \to \frac{1}{\varepsilon}\rho|e| > 1 \to 1 - \frac{1}{\varepsilon}\rho|e| < 0 \to \rho|e|\left(1 - \frac{1}{\varepsilon}\rho|e|\right) < 0 \tag{41}$$

$$\dot{V}(x) \leq -ke^2 + \rho|e|\left(1 - \frac{1}{\varepsilon}\rho|e|\right) \leq -ke^2 \leq 0 \tag{42}$$

2) $\rho|e| < \varepsilon$

$$\rho|e| \leq \varepsilon \to \frac{1}{\varepsilon}\rho|e| \leq 1 \to 0 \leq 1 - \frac{1}{\varepsilon}\rho|e| \leq 1 \to \rho|e|\left(1 - \frac{1}{\varepsilon}\rho|e|\right) \leq \rho|e| \leq \varepsilon \tag{43}$$

$$\dot{V}(x) \leq -ke^2 + \varepsilon \tag{44}$$

Bring Formula (35) into Formula (44) to get

$$\dot{V}(x) \leq -2kV(x) + \varepsilon \tag{45}$$

To solve the differential equation inequality (45), $S(t) > 0$ is introduced to make the differential equation inequality become an equality:

$$\dot{V}(x) + 2kV(x) + S(t) = \varepsilon \tag{46}$$

The differential equation in Equation (46) can be solved as

$$\begin{aligned} V(t) = V(0)\exp(-2kt) - \exp(-2kt)\int_0^t \exp(-2k\tau)S(\tau)d\tau \\ + \varepsilon\exp(-2kt)\int_0^t \exp(2k\tau)d\tau \end{aligned} \tag{47}$$

The error $e(t)$ Equation (48) obtained by simplification is

$$|e(t)| \leq \left[|e(0)|\exp(-2kt) + \frac{\varepsilon}{k}(1-\exp(-2kt))\right]^{\frac{1}{2}} \tag{48}$$

When $t \to \infty$

$$\lim_{t\to\infty} |e(t)| \leq \sqrt{\frac{\varepsilon}{k}} \tag{49}$$

The final error function satisfies Equation (49) and remains stable within a certain range, which is called GUUB (Globally Uniformly Ultimately Bounded) and globally uniformly bounded.

4. **Carsim/Simulink Joint Simulation Analysis and Main Results.** Based on the vehicle dynamics model in Section 2, the failure cases analysis, and the fault-tolerant control strategy designed in Section 3, a simulation model is constructed to simulate and analyze the vehicle's state under various braking failure cases. Synovial control achieves robust control against system uncertainties and external disturbances by designing a switching surface (the sliding surface) that forces the system's state trajectory to remain on and slide along this surface. Characterized by its strong anti-interference capability and rapid dynamic response, we therefore compared the synovial control algorithm with the fault-tolerant control algorithm proposed in Section 3.

4.1. **Simulation analysis of single-wheel failure.** The left front wheel is taken as an example to examine the variations in vehicle state parameters under different levels of brake failure (10%, 50%, and 100%).

(i) The ground adhesion coefficient is 0.75, the degree of failure is 10%, the initial speed is 80 km/h, and the emergency braking condition is linear braking. As can be seen from Figure 7, after applying fault-tolerant control, the vehicle's yaw rate fluctuation amplitude is reduced to around 0.1 deg/s, the heading angle remains around 0.1, the lateral deviation distance is nearly zero, and the braking distance is significantly shorter compared to other scenarios.

(ii) The ground adhesion coefficient is 0.75, the degree of failure is 50%, the initial speed is 80 km/h, and the emergency braking condition is linear braking. As observed in Figure 8, under this operating condition, the implementation of fault-tolerant control stabilizes the vehicle's yaw rate fluctuation around 3.8 deg/s, maintains the heading angle at approximately 1.3 degrees, reduces the lateral deviation distance to 0.02 m, and significantly shortens the braking distance.

(iii) The ground adhesion coefficient is 0.75, the degree of failure is 100%, the initial speed is 80 km/h, and the emergency braking condition is linear braking. As depicted in Figure 9, when a single wheel experiences severe failure, the vehicle equipped with fault-tolerant control maintains a yaw rate fluctuation of approximately 7.3 deg/s, a heading angle deviation of around 6 degrees, and a lateral deviation of about 0.6 meters. In contrast, the uncontrolled vehicle exhibits a substantial heading angle deviation of nearly 200 degrees, leading to a lateral deviation of up to 12 meters, resulting in severe braking deviation and a potential spin-out.

The above results show that a fault-tolerant control strategy significantly improves vehicle stability and shortens braking distance when left front wheel single-wheel failure occurs during straight-line braking.

4.2. **Simulation analysis of two-wheel failure.** The two-wheel failure case is examined using two scenarios: front-axle two-wheel failure and same-side two-wheel failure. The analysis aims to verify the changes in the vehicle's driving state parameters under varying degrees of brake failure (5%, 10%, 35%, 50%, 95%, and 100%).

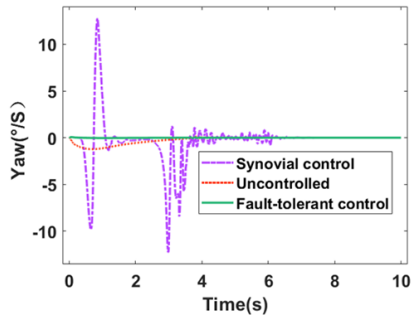

(a) Comparison of yaw velocity

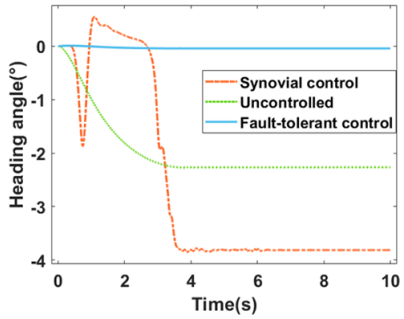

(b) Comparison of heading angle

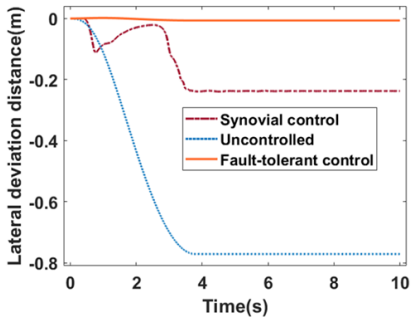

(c) Comparison of lateral deviation distance

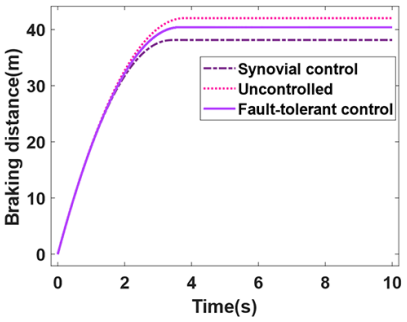

(d) Comparison of braking distance

FIGURE 7. Comparison curves of the vehicle's driving state parameters at 10% brake force failure

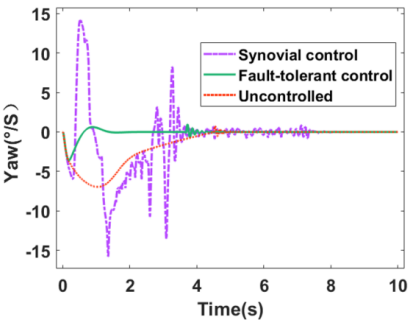

(a) Comparison of yaw velocity

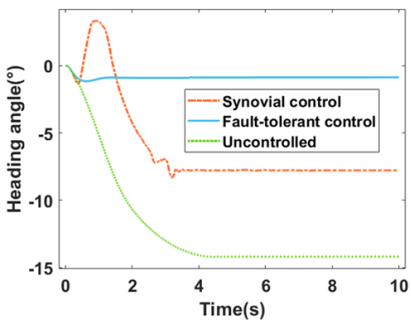

(b) Comparison of heading angle

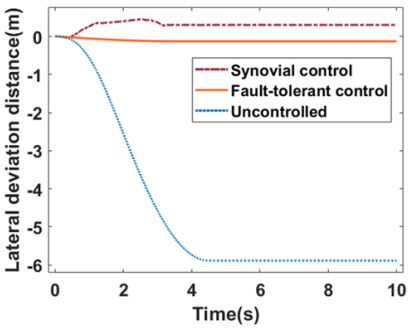

(c) Comparison of lateral deviation distance

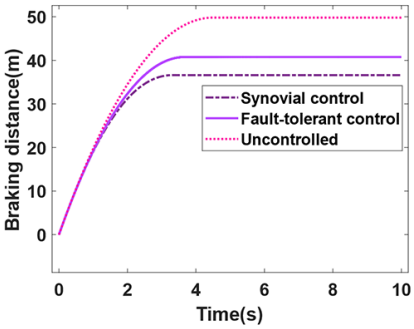

(d) Comparison of braking distance

FIGURE 8. Comparison curves of the vehicle's driving state parameters at 50% brake force failure

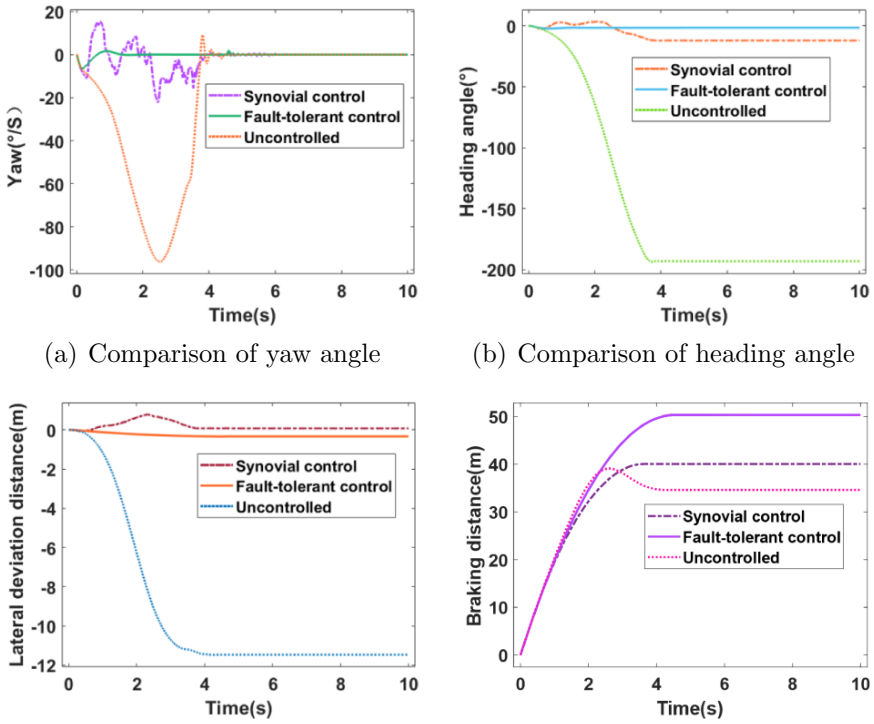

(a) Comparison of yaw angle

(b) Comparison of heading angle

(c) Comparison of lateral deviation distance

(d) Comparison of braking distance

FIGURE 9. Comparison curves of the vehicle's driving state parameters at 100% brake force failure

4.2.1. *Simulation analysis of the two-wheel failure on the front axle.*

(i) The following parameters are set for the simulation: a ground adhesion coefficient of 0.75, a 10% failure in the left front wheel, a 5% failure in the right front wheel, an initial speed of 80 km/h, mild failure cases, and emergency braking cases for straight-line braking.

As illustrated in Figure 10, the vehicle equipped with fault-tolerant control maintains a yaw rate of approximately 0.1 deg/s, with its heading angle remaining virtually unchanged and lateral deviation nearly zero, resulting in a shorter braking distance.

(ii) The following parameters are set for the simulation: a ground adhesion coefficient of 0.75, a 50% failure in the left front wheel, a 35% failure in the right front wheel, an initial speed of 80 km/h, mild failure cases, and emergency braking cases for straight-line braking. As shown in Figure 11, the vehicle with fault-tolerant control exhibits a yaw rate of approximately 1 deg/s, a heading angle deviation of around 0.4 degrees, and a lateral deviation of 0.19 meters. The braking distance is significantly reduced compared to vehicles without such control.

(iii) The following parameters are set for the simulation: a ground adhesion coefficient of 0.75, a 100% failure in the left front wheel, a 35% failure in the right front wheel, an initial speed of 80 km/h, severe failure cases, and emergency braking cases for straight-line braking. As depicted in Figure 12, the yaw rate of the vehicle equipped with fault-tolerant control is around 4 deg/s, with a heading angle deviation of approximately 2 degrees and a lateral deviation of roughly 0.6 meters. In contrast, the uncontrolled vehicle experiences a significant heading angle deviation of about 23 degrees, resulting in a lateral deviation of up to 16 meters, indicating a severe braking deviation.

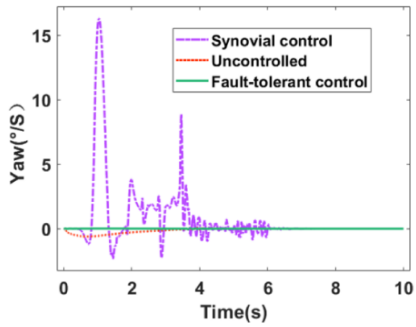

(a) Comparison of yaw angle

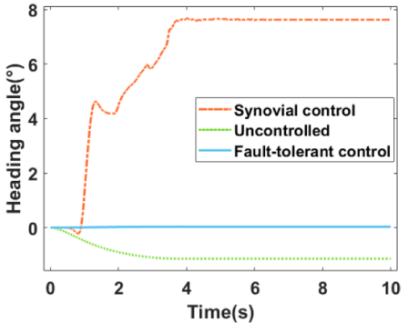

(b) Comparison of heading angle

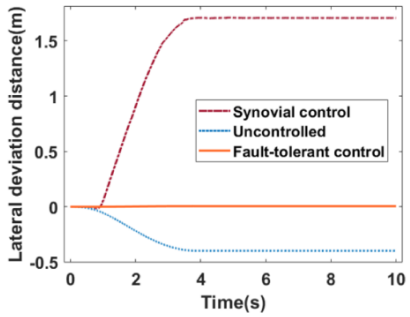

(c) Comparison of lateral deviation distance

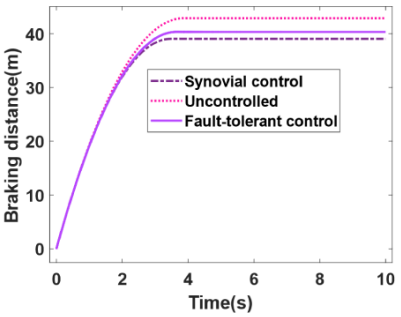

(d) Comparison of braking distance

FIGURE 10. Comparison curves of the vehicle's driving state parameters during mild brake failure

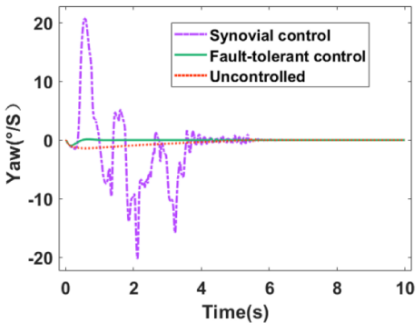

(a) Comparison of yaw angle

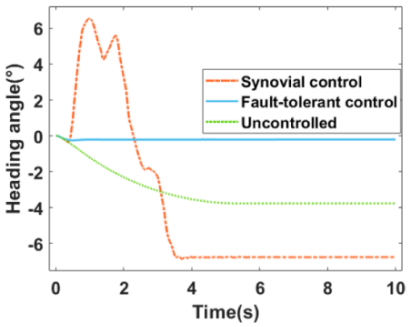

(b) Comparison of heading angle

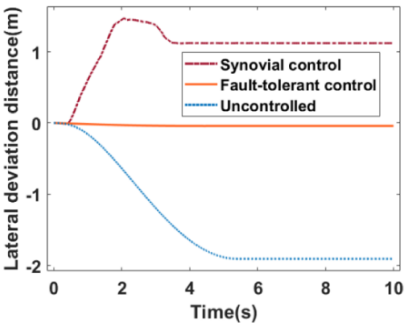

(c) Comparison of lateral deviation distance

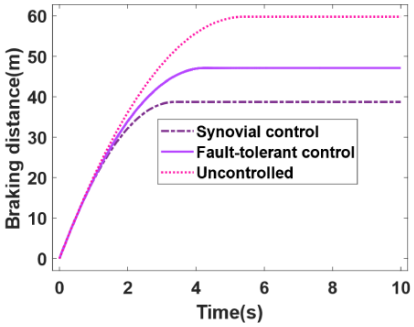

(d) Comparison of braking distance

FIGURE 11. Comparison curves of the vehicle's driving state parameters during moderate brake failure

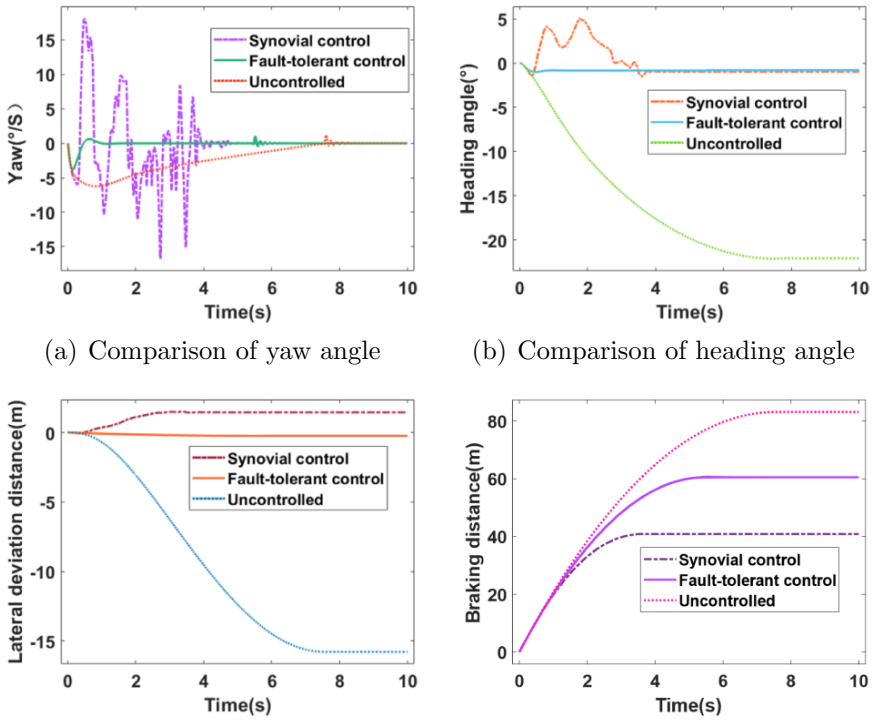

(a) Comparison of yaw angle (b) Comparison of heading angle

(c) Comparison of lateral deviation distance (d) Comparison of braking distance

FIGURE 12. Comparison curves of the vehicle's driving state parameters during severe brake failure

The above three condition plots show that a fault-tolerant control strategy significantly improves vehicle stability and reduces braking distance when handling front axle two-wheel failure under straight-line brakes.

4.2.2. *Simulation analysis of two-wheel failure on the same side.*

(i) For the failure of two wheels on the left side, the following parameters are set: a road ground adhesion coefficient of 0.75, a 10% failure in the left front wheel, a 5% failure in the left rear wheel, an initial speed of 80 km/h, mild failure cases, and emergency braking cases for straight-line braking.

As shown in Figure 13, the vehicle with fault-tolerant control exhibits a yaw rate of approximately 0.46 deg/s, a heading angle deviation of around 0.18 degrees, and a lateral deviation of 0.08 meters. Additionally, the braking distance is shorter compared to vehicles without such control.

(ii) For the failure of two wheels on the left side, the following parameters are set: a ground adhesion coefficient of 0.75, a 10% failure in both the left front and left rear wheels, an initial speed of 80 km/h, mild failure cases, and emergency braking cases for straight-line braking.

As can be seen from Figure 14, the yaw rate of the vehicle with fault-tolerant control is around 0.48 deg/s; the vehicle's heading angle is around 0.2 degrees, the side slip distance is 0.1 m, and the braking distance is shorter.

(iii) For the failure of two wheels on the left side, the following parameters are set: a ground adhesion coefficient of 0.75, a 100% failure in the left front wheel, a 95% failure in the right front wheel, an initial speed of 80 km/h, severe failure cases, and emergency braking cases for straight-line braking.

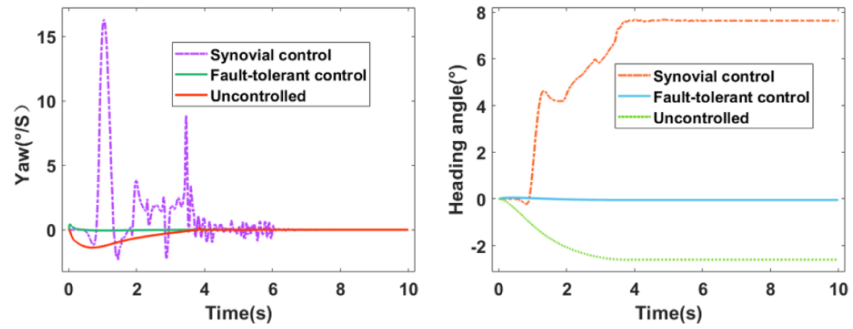

(a) Comparison of yaw angle

(b) Comparison of heading angle

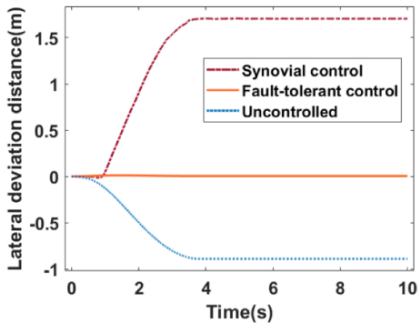

(c) Comparison of lateral deviation distance

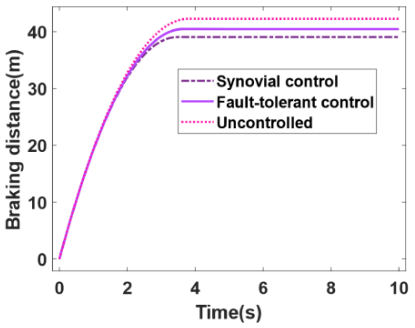

(d) Comparison of braking distance

FIGURE 13. Comparison curves of the vehicle's driving state parameters during mild brake failure

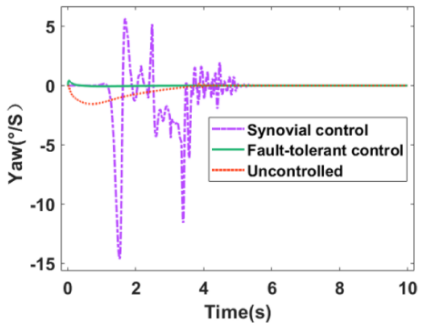

(a) Comparison of yaw angle

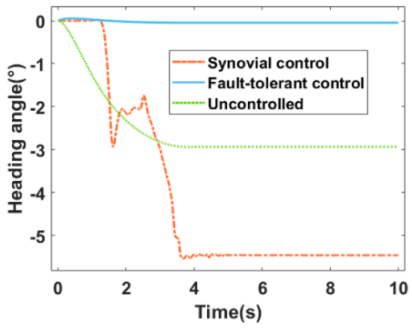

(b) Comparison of heading angle

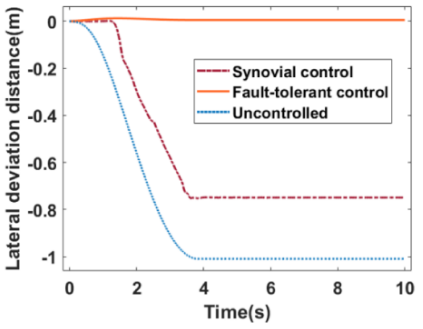

(c) Comparison of lateral deviation distance

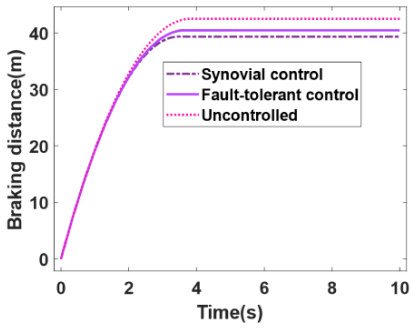

(d) Comparison of braking distance

FIGURE 14. Comparison curves of the vehicle's driving state parameters during moderate brake failure

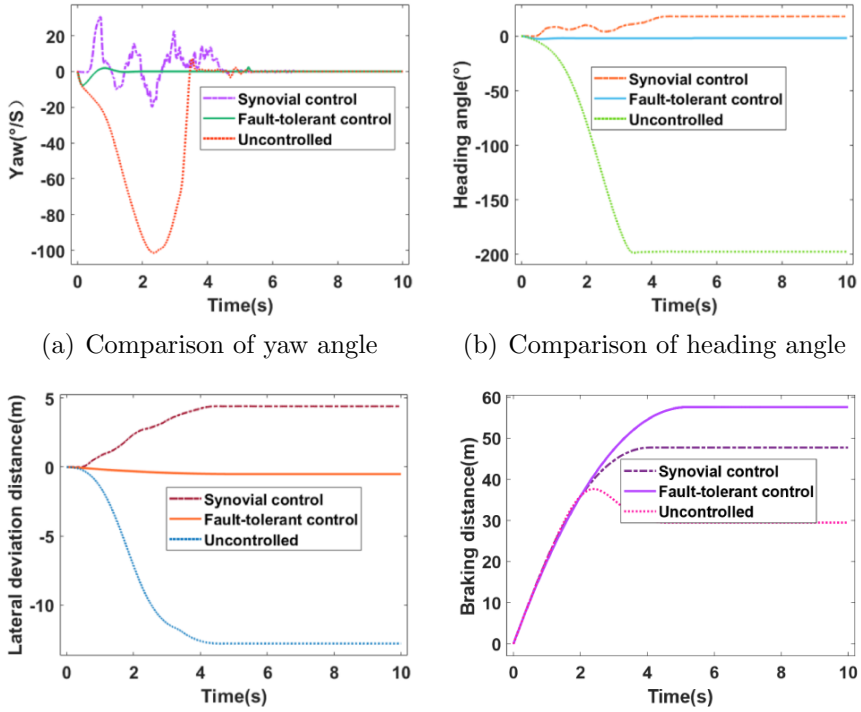

(a) Comparison of yaw angle (b) Comparison of heading angle

(c) Comparison of lateral deviation distance (d) Comparison of braking distance

FIGURE 15. Comparison curves of the vehicle's driving state parameters during severe brake failure

As illustrated in Figure 15, the yaw rate of the vehicle equipped with fault-tolerant control is maintained at approximately 10 deg/s, while its heading angle remains around 10 degrees, and the lateral deviation distance is kept to a mere 1.3 m. In stark contrast, the uncontrolled vehicle experiences a significant heading angle deviation of roughly 200 degrees, resulting in a lateral deviation distance of approximately 14.5 m, indicating severe braking instability and potentially even a spin-out.

The simulation results demonstrate that when the vehicle without fault-tolerant control experiences an EMB braking failure, it results in insufficient braking force, poor stability, significant deviation, ultimately leading to nearly a 360-degree rotation of the body. The fault-tolerant control strategy in this paper effectively contributes to body stability and braking safety during braking, as demonstrated by the comparison of the braking distance, yaw velocity, and lateral deviation distance.

5. **Conclusions.** This paper examines a total of 126 failure cases. Specifically, we analyze the variations in vehicle force, mechanical braking force, and electric mechanism force during straight-line braking under 63 different failure scenarios. These include single-wheel failure, front axle two-wheel failure, diagonal two-wheel failure on the left side, and left-side two-wheel failure.

We design fault-tolerant control strategies for different failure conditions, based on the force analysis of the failure cases and the braking force changes of each brake and motor, to enhance the vehicle's stability and safety during braking. The designed strategies are simulated and verified by the Carsim/Simulink joint simulation platform. The results show that the fault-tolerant control strategy designed in this paper can largely improve the braking stability and safety of the vehicle during braking failure, as can be seen from the vehicle's yaw velocity, heading angle, lateral deviation distance, and braking distance.

This paper focuses on brake failure and designs fault-tolerant control algorithms to compensate for the lost braking force by utilizing healthy brakes and motors. However, motor failure is not considered in this study. Future research should further explore the impact of motor failure and develop corresponding fault-tolerant strategies.

Acknowledgment. This work is partially supported by Chongqing Natural Science Foundation general project under Grant CSTB2023NSCQ-MSX0418. The authors also gratefully acknowledge the helpful comments and suggestions of the reviewers, which have improved the presentation.

REFERENCES

[1] Y. Kang, *Sensor Fault Diagnosis and Fault Tolerant Control of Integrated Brake Control System Based on Functional Safety Analysis*, Master Thesis, Jilin University, 2022.

[2] K. Xiao, *Game-Based Four-Wheel Independent Driving Vehicle Fault-Tolerant and Longitudinal & Lateral Motion Integrated Control*, Master Thesis, Chongqing University, 2020.

[3] B. Zhu, R. Dang and J. Zhao, Fault-tolerant control of current sensors in redundant electronic braking system for an intelligent vehicle, *China Journal of Highway and Transport*, vol.36, no.4, pp.249-260, 2023.

[4] R. Dang, *Research on Sensor Fault Diagnosis and Fault-Tolerant Control of Integrated Brake Control System*, Master Thesis, Jilin University, 2023.

[5] K. Patan and M. Patan, Sensor fault-tolerant control design for magnetic brake system, *Sensors*, vol.20, no.16, pp.1-18, 2020.

[6] Y. Yuan, *The Development and Fault Tolerance Control of Vehicular Regenerative By-Wire Braking Systems*, Ph.D. Thesis, Tsinghua University, 2019.

[7] P. Qie, *Research on Composite Braking and Fault Tolerant Control of Multi-Axle Independent Electric Drive Vehicles*, Master Thesis, Jilin University, 2023.

[8] K. Patan and M. Patan, Actuator fault-tolerant iterative learning control of the magnetic brake system, *The 11th IFAC Symposium on Fault Detection, Supervision and Safety for Technical Processes SAFEPROCESS 2022*, Pafos, Cyprus, vol.55, no.6, pp.266-271, 2022.

[9] R. Raveendran, K. B. Devika and S. C. Subramanian, Brake fault identification and fault-tolerant directional stability control of heavy road vehicles, *IEEE Access*, vol.8, pp.169229-169246, 2020.

[10] X. Cao, Y. Tian, X. Ji and B. Qiu, Fault-tolerant controller design for path following of the autonomous vehicle under the faults in braking actuators, *IEEE Transactions on Transportation Electrification*, vol.7, no.4, pp.2530-2540, 2021.

[11] J. Yuan, J. Zhang and W. Liu, Fault-tolerant control of regenerative braking system on in-wheel motors driven electric vehicles, *SAE Technical Paper Series: SAE International*, 2020.

[12] X. Wang, S. Wang, S. An and H. Liu, An adaptive disturbance suppression-based fault-tolerant control approach against the control surface faults, *International Journal of Innovative Computing, Information and Control*, vol.19, no.1, pp.213-227, 2023.

[13] Y. Yu, Y. Wang, D. Xu, Z. Dou and M. Yang, Research on charging and discharging strategy of electric vehicles in park micro-grid based on pigeon-inspired optimization algorithm, *International Journal of Innovative Computing, Information and Control*, vol.19, no.3, pp.721-735, 2023.

[14] X. Liu, H. Zhang and J. Zhao, Resilient distributed event-triggered platooning control of connected vehicles under denial-of-service attack, *IEEE Transactions on Intelligent Transportation Systems*, vol.24, no.6, pp.6191-6202, 2023.

[15] X. Li, Y. Zhang and Z. Chen, Fault-tolerant control of distributed drive electric vehicles under brake-by-wire system failures, *IEEE Transactions on Vehicular Technology*, vol.71, no.5, pp.4321-4333, 2022.

[16] H. Wang, J. Liu and K. Li, Cooperative fault-tolerant control for in-wheel motor driven EVs with electro-mechanical brake actuator failures, *Control Engineering Practice*, vol.131, 105407, 2023.

[17] Z. Zhang, S. Yu and T. Song, Resilient torque distribution strategy for distributed drive electric vehicles under brake system faults, *IEEE/ASME Transactions on Mechatronics*, vol.26, no.4, pp.2135-2145, 2021.

[18] Q. Guo, L. Zhang and Y. Wang, Intelligent fault-tolerant control of electric vehicles with hub motors and EMBs using deep reinforcement learning, *Mechanical Systems and Signal Processing*, vol.186, 109832, 2023.

[19] Q. Chen, Y. Jia and Y. Che, Integrated chassis control of distributed drive EVs considering EMB failures and actuator saturation, *Chinese Journal of Mechanical Engineering*, vol.35, no.1, pp.1-12, 2022.
[20] T. Yi, *Compilation of National Automobile Standards Body and Chassis*, China National Standards Publishing House, Beijing, 1999.
[21] L. Huang, Design and validation of a MATLAB-based dual closed-loop DC speed control system, *Equipment Manufacturing Technology*, vol.2023, no.8, pp.48-51, 2023.
[22] Y. Sun, *Research on Brake Stability Compensation Control of Distributed Drive Electric Vehicle with Brake Failure*, Master Thesis, Yanshan University, 2021.

Author Biography

Xin Ye (IEEE Member) received the B.Sc. degree in Mechanical Engineering from Chongqing University, China, 2004; the Ph.D. degree in Vehicle Engineering from Chongqing University, China, 2011.

She is currently a professor at the School of Vehicle Engineering, Chongqing University of Technology, China. Her research fields include new energy and intelligent vehicle integrated control, intelligent algorithm research and so on. She has led 3 national projects and published over 20 papers in journals and conference.

Xingang Li graduated from the School of Intelligent Manufacturing and Vehicle Engineering of Sichuan Institute of Industrial Science and Technology, China, in 2021 with a bachelor's degree in Vehicle Engineering. He received his master's degree in Vehicle Engineering from Chongqing University of Technology, China, in 2024.

His research focused on regenerative braking and fault-tolerant control strategies for new energy vehicles, including brake-by-wire systems, regenerative braking control strategies, and motor and brake co-control, during his master's program. He is currently working as a Development Engineer at Geely Automobile Research Institute (Ningbo) Co., Ltd.

Xiaoxuan Cheng received the bachelor's degree in Vehicle Engineering from the School of Mechanical Engineering at Shenyang University, China, in 2022.

She is currently pursuing her master's degree in Vehicle Engineering at Chongqing University of Technology, China. Her research mainly focused on intelligent vehicle control, including traffic flow modeling, vehicle queue modeling and controller setup during her master's program.

Qi Cao received his Ph.D. degree in Computer Science from Chongqing University, China, in 2010. He was ever a visiting scholar in the Department of Computer Science and Engineering in the Tandon School of Engineering at the New York University, USA, and a postdoctoral researcher in the Department of Management Science and Engineering in the Business School at the Nankai University, China. And now he is a professor at the Joint Logistics Support Force University of Engineering, China. His research interests include computer modelling and simulation, nonlinear constrained optimization, pattern recognition and machine learning.

Zhongping Kang received the bachelor's degree in Vehicle Engineering from the School of Mechanical and Intelligent Manufacturing at Jiujiang University, China, in 2023. He is currently pursuing his master's degree in Vehicle Engineering at Chongqing University of Technology, China. His research mainly focused on fault-tolerant control for communication failures in intelligent and connected vehicle platoons, encompassing modeling of intelligent and connected vehicle platoons, modeling of communication failures, and controller design.